
INTEGRATION OF LEAKY-INTEGRATE-AND-FIRE-NEURONS IN DEEP LEARNING ARCHITECTURES

RUNNING TITLE: LIF UNITS IN DEEP LEARNING

Richard C. Gerum

Biophysics Group, Department of Physics
Friedrich Alexander University Erlangen-Nürnberg (FAU), Germany

Achim Schilling

Experimental Otolaryngology,
Neuroscience Lab, University Hospital Erlangen, Germany
Cognitive Computational Neuroscience Group
at the Chair of English Philology and Linguistics,
Friedrich-Alexander University Erlangen-Nürnberg (FAU), Germany

January 11, 2022

Corresponding author:

Dr. Achim Schilling
Neuroscience Group
Experimental Otolaryngology
Friedrich-Alexander University of Erlangen-Nürnberg
Waldstrasse 1
91054 Erlangen, Germany
Phone: +49 9131 8543853
E-Mail: achim.schilling@uk-erlangen.de

ABSTRACT

Up to now, modern Machine Learning is mainly based on fitting high dimensional functions to enormous data sets, taking advantage of huge hardware resources. We show that biologically inspired neuron models such as the Leaky-Integrate-and-Fire (LIF) neurons provide novel and efficient ways of information encoding. They can be integrated in Machine Learning models, and are a potential target to improve Machine Learning performance.

Thus, we derived simple update-rules for the LIF units from the differential equations, which are easy to numerically integrate. We apply a novel approach to train the LIF units supervisedly via backpropagation, by assigning a constant value to the derivative of the neuron activation function exclusively for the backpropagation step. This simple mathematical trick helps to distribute the error between the neurons of the pre-connected layer. We apply our method to the IRIS blossoms image data set and show that the training technique can be used to train LIF neurons on image classification tasks. Furthermore, we show how to integrate our method in the KERAS (tensorflow) framework and efficiently run it on GPUs. To generate a deeper understanding of the mechanisms during training we developed interactive illustrations, which we provide online.

With this study we want to contribute to the current efforts to enhance Machine Intelligence by integrating principles from biology.

Introduction

The interest in „Neuroscience inspired AI“ has rapidly grown over the last years (Hassabis et al., 2017). There are major reasons for this development. Although traditional Machine Learning algorithms have been massively improved by the collection of huge data sets (Russakovsky et al., 2015) and the development of modern hardware components (Steinkraus et al., 2005; Sheng and Zhou, 2017), certain issues remain unsolved by these algorithms. Up to now, these algorithms are—in contrast to our brain—highly specialized on a given task. We were not yet able to develop algorithms with general intelligence (Shevlin et al., 2019; Pontes-Filho and Nichele, 2019). Our nervous system has the ability to perform sensory tasks with enormous precision, such as the detection of very low stimuli in the eye (Field et al., 2019; Rieke and Baylor, 1998) or very small pressure differences in the ear and on the other hand is able to process and understand complex story plots (Mar, 2004; Tenenbaum et al., 2006). Thus, we do not need huge hardware components but are limited to approximately 10^{11} neurons (Herculano-Houzel, 2009), which perform these tasks in a very efficient way.

Information can be processed faster and more efficiently in the brain, as spiking neural networks can encode data in different spatio-temporal patterns (Thorpe et al., 2001; Perkel and Bullock, 1968; Krauss et al., 2018; Gross and Kowalski, 1999). Thus, the brain does not simply count spikes (rate codes) but exploits the temporal dynamics of these spikes (Koopman et al., 2003) and uses spontaneous spiking and neural noise to enhance sensory processing (Schilling et al., 2020; Krauss et al., 2017, 2016).

Different biological inspired neuron models have been developed such as the Hodgkin-Huxley or the Fitzhugh-Nagumo neuron (Hodgkin and Huxley, 1952; Izhikevich and FitzHugh, 2006), but they are rarely integrated in Machine Learning applications.

Biologically inspired Leaky-Integrate-and-Fire (LIF) neurons (Burkitt, 2006) are an interesting target for Machine Learning models to potentially improve performance and increase interpretability on the one hand ("Neuroscience inspired AI" (Hassabis et al., 2017)) and to create models for biology on the other hand ("Cognitive Computational Neuroscience" (Kriegeskorte and Douglas, 2018)).

Due to these properties of spiking networks and especially LIF units much effort has been undertaken to train LIF neuron networks supervisedly via backpropagation.

In 2000 an interesting approach for training LIF networks via backpropagation was introduced, named SpikeProp, which was several times improved and further developed (Bohte et al., 2000; Schrauwen and Van Campenhout, 2004a,b). The basic idea of the algorithm is that not spiking patterns are learned, but desired spike times are defined as learning targets. In other approaches the input encoding is restricted to only one spike per neuron (Kheradpisheh and Masquelier, 2019), meaning that the information is encoded in the time to first spike. Furthermore, some researchers use approximated derivatives in the gradient descent method to account for the discontinuities of the LIF neurons (Wu et al., 2018; Lee et al., 2020). Furthermore, some studies show that Long-Short-Term-Memory (LSTM) units (Hochreiter and Schmidhuber, 1997) can also be trained, so that they behave like spiking neurons (Koopman et al., 2003; Pozzi et al., 2018; Rezaabad and Vishwanath, 2020). This insight helps to use existing pipelines to train spiking neural networks. In this context, it has to be stated that in recent studies artificial spiking neural networks are more and more often compared to biological systems to understand and rebuild them (Kim et al., 2019). Additionally, the spiking neural networks are an interesting target for energy efficient computation on small computer chips (Lee et al., 2020).

We here introduce a very direct way to train LIF neurons using backpropagation. Thus, we manually fix the derivative of the LIF neuron only within the backpropagation step and thus the error contributing to a certain spike can be distributed over the neurons of the pre-connected layer. The study is structured as follows. We firstly illustrate and explain the function of LIF neurons. In a second step, we introduce our method to train LIF units with backpropagation. We prove the validity of our approach by the application of the method in hybrid neural networks trained on an image classification task using the IRIS data set (Nilsback and Zisserman, 2008). The study comes along with interactive versions of most of the figures, which help the reader to gain a better understanding of the mechanisms within spiking neural networks.

Methods

All simulations were run on a standard Desktop PC equipped with a Nvidia TitanXp Gpu device. The simulations were written in Python using Keras (Chollet, 2018) and Tensorflow (Abadi et al., 2016) for Machine Learning and Numpy (Walt et al., 2011) for further evaluations and interfaces. The visualization of the data was done in Javascript using the D³-library (Bostock et al., 2011) and in Python using Matplotlib (Hunter, 2007) and Pylustrator (Gerum, 2020).

Thus, we provide interactive plots in an open github-repository. This interactive plots should help to gain a deeper understanding of the mechanisms described in the paper. A link to the repository is provided in the figure captions.

Results

Leaky Integrate and Fire Neurons (LIF)

As described above the Leaky-Integrate-and-Fire (LIF) neuron model is a simple spiking neuron model based on one single differential equation. The idea is that the neuron sums up all input currents, increases its' membrane potential and produces a spike if a certain threshold is reached (see Fig. 1). The leak term causes a continuous decrease of the membrane potential and thus prevents long-range correlations.

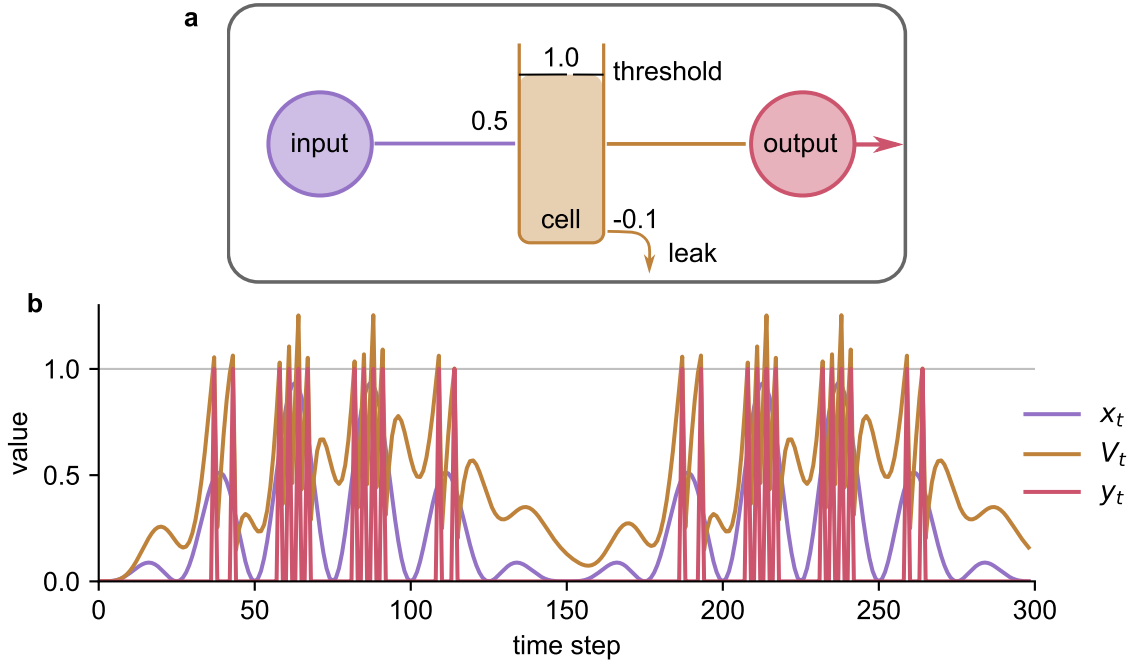


Figure 1: **The response of the leaky integrate and fire neurons.** **a**, illustration of the data flow in a LIF unit. **b**, the response of the LIF unit to a given input signal. The cell (V_t , orange) integrates the input (x_t , purple) until the internal state exceeds the threshold (gray line). Then it outputs a spike (y_t , red). The leak term lets the cell state decay over time. With the parameters: $w_{\text{input}} = 0.5$, $w_{\text{leak}} = 0.1$, $V_{\text{thresh}} = 1.0$. For interactive version see: https://rgerum.github.io/paper_spiking_machine_intelligence/#lif_unit

The leaky integrate and fire (LIF) neuron's (Koch et al., 1998) membrane potential V_m is described by the following differential equation:

$$I(t) - \frac{V_m(t)}{R_m} = C_m \cdot \dot{V}_m(t) \quad (1)$$

(with the input current $I(t)$, the membrane resistance R_m , and the membrane capacity C_m .)

When the membrane potential exceeds a threshold V_{th} , a spike in form of a delta function $\delta(t)$ is emitted and the membrane potential is reset to 0. To simulate the response of a LIF neuron, this differential equation has to be integrated. The standard integration method is the Euler integration (Atkinson, 1989), which we used for this approach. First, the differential equation is solved for $\dot{V}_m(t)$

$$\dot{V}_m(t) = \frac{I(t)}{C_m} - \frac{V_m(t)}{R_m C_m} \quad (2)$$

This differential equation can be reformulated in a recursive manner (for one Euler step).

$$V_{t+1} = V_t + (C_m^{-1} \cdot x_t - V_t \cdot R_m^{-1} C_m^{-1}) \cdot \Delta t \quad (3)$$

(with the time step delta Δt , and the $I(t)$ now renamed x_t .) We extend the update equation to include the spiking when the threshold has been reached and the resetting of V_{t+1} after the spike.

$$\tilde{V}_{t+1} = V_t + (C_m^{-1} \cdot x_t - V_t \cdot R_m^{-1} C_m^{-1}) \cdot \Delta t \quad (4)$$

$$y_{t+1} = \Theta(\tilde{V}_{t+1} - V_{\text{thresh}}) \quad \text{spiking} \quad (5)$$

$$V_{t+1} = V_m \cdot \Theta(-\tilde{V}_{t+1} + V_{\text{thresh}}) \quad \text{resetting} \quad (6)$$

Where $\Theta(x)$ is the Heaviside step function. The parameters can be renamed as follows:

$$C_m^{-1} \Delta t = w_{\text{input}} \quad (7)$$

$$R_m^{-1} C_m^{-1} \cdot \Delta t = w_{\text{leak}} \quad (8)$$

Without loss of generality, V_{thresh} can be fixed to 1, as the scaling can be absorbed in w_{input} . The update rule of the LIF unit can be summarized as follows:

$$V_t = w_{\text{input}} \cdot x_t + (1 - w_{\text{leak}}) \cdot V_{t-1} \cdot \Theta(V_{\text{thresh}} - V_{t-1}) \quad (9)$$

$$y_t = \Theta(V_t - V_{\text{thresh}}) \quad (10)$$

These equations can e.g. be used to analytically calculate the firing rates r of the LIF neurons (for calculation see Suppl. Fig. S1). The firing rates are an important property for many Machine Learning algorithms (Dominguez-Morales et al., 2016).

$$r = 1/\text{ceil} \left(\frac{\ln \left(1 - \frac{V_{\text{thresh}}}{I} \cdot \frac{w_{\text{leak}}}{w_{\text{input}}} \right)}{\ln(1 - w_{\text{leak}})} - 1 \right) \quad (11)$$

Here, $\text{ceil}(x)$, denotes the ceiling of a number, i.e. rounding up to the closest integer.

Deep Learning with LIF Neurons

We show how the LIF neurons can be integrated in standard Machine learning applications for image classification.

LIF Neurons and Multidimensional Data

When the LIF neurons are applied to multi-dimensional data such as an image an efficient representation is needed to optimize LIF neurons for our standard hardware and software architectures. The image, which we feed to the LIF units has N rows and M columns ($N \times M$). However, we regard the image as serial data set, where the time axis corresponds to the x-axis of the image. Thus, the input of the LIF neurons consists of an N -dimensional vector for each of the M time steps. Therefore, also V_t and y_t are N -dimensional vectors. Thus, when an image is fed to a LIF unit as described above (input image see Fig. 2a) it is transformed to "voltage fluctuations" in the LIF unit (see Fig. 2b) and output spiking patterns (see Fig. 2c).

The model can be extended by the use of several LIF units with different w_{input} and w_{leak} (see eq. 10). This would make w_{input} and w_{leak} a vector instead of a scalar and the scalar product would transform into a tensor product. This is an efficient representation, which can easily be optimized for and run on GPUs.

Calculation of the Gradient

The standard method to supervisedly train neural networks on a classification task is to minimize a loss function $L(y_{\text{out}}, y_{\text{desired}})$. It is a measure of the dissimilarity between the desired output and the output of the neural network y_{out} calculated by forward propagation. For example in a classification task with a softmax output, the loss function usually is the cross-entropy. This loss function is minimized using a gradient descent algorithm. The gradient descent works by adding the negative gradient multiplied with the learning rate γ to the weights, which have to be optimized.

$$\Delta W = -\gamma \cdot \frac{dL}{dW} \quad (12)$$

To illustrate the calculation of the gradient, we use an example architecture, consisting of two fully-connected layers and a LIF layer in between (see Fig. 3).

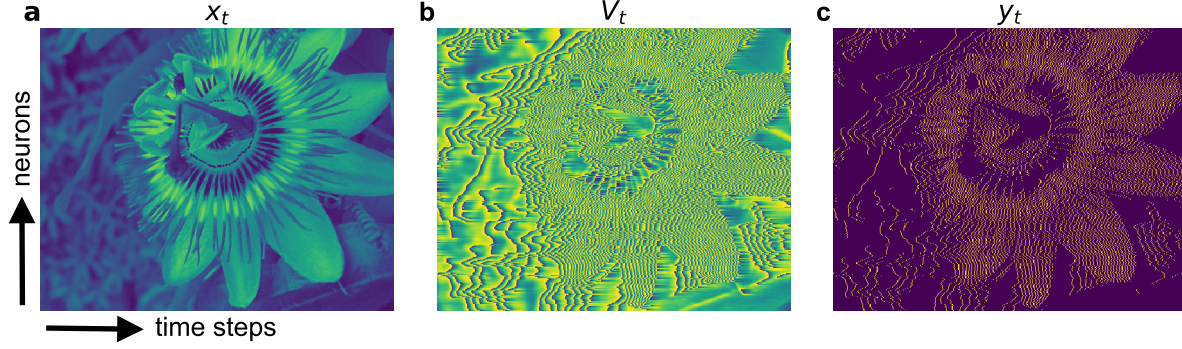


Figure 2: **Image processed column-wise by a LIF layer.** The figure shows the input (a), internal state (b), and the output (c) of the LIF layer. For interactive version see: https://rgerum.github.io/paper_spiking_machine_intelligence/#lif_image_processing

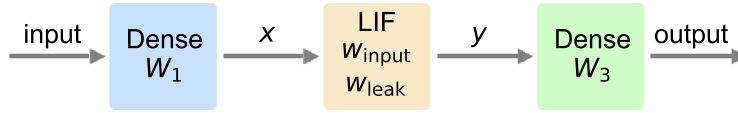


Figure 3: **Example network architecture**

Example neural network architecture used to illustrate the gradient descent algorithm.

To calculate the update of the weights W_1 , we have to calculate the gradient $\frac{dL}{dW_1}$.

$$\frac{dL}{dW_1} = \frac{\partial L}{\partial y_{out}} \cdot \frac{\partial y_{out}}{\partial y} \cdot \frac{\partial y}{\partial x} \cdot \frac{dx}{dW_1} \quad (13)$$

The term $\frac{\partial y}{\partial x}$ is the derivative of the LIF output as a function of the LIF input. If this derivative is 0 the weights of the first layer W_1 cannot be trained.

$$V_t = w_{input} \cdot x_t + (1 - w_{leak}) \cdot V_{t-1} \cdot \Theta_2(V_{thresh} - V_{t-1}) \quad (14)$$

$$y_t = \Theta_1(V_t - V_{thresh}) \quad (15)$$

However, this is exactly the case, as the LIF equations contain two Θ functions. To better reference them, we call the Θ function for generation of the output spike Θ_1 and the Θ function for resetting the membrane potential Θ_2 . As the Θ function is a completely flat function (except at 0), its' gradient is 0 at all points, therefore reducing all gradients to 0. Thus, no gradient can enter or pass the LIF cell. One possibility to overcome this problem would be to smooth the Θ functions. But a more elegant solution, that does not affect the forward pass, is to just redefine the gradient of the LIF unit. The derivative with respect to the inputs can be written as follows:

$$\frac{\partial y_t}{\partial x_t} = \frac{\partial y_t}{\partial V_t} \frac{\partial V_t}{\partial x_t} = \Theta_1'(V_t - V_{thresh}) \cdot w_{input} \quad (16)$$

$$\frac{\partial y_t}{\partial x_{t-1}} = \frac{\partial y_t}{\partial V_t} \frac{\partial V_t}{\partial V_{t-1}} \frac{\partial V_{t-1}}{\partial x_{t-1}} \quad (17)$$

$$= \Theta_1'(V_t - V_{thresh}) \cdot (1 - w_{leak}) \cdot [\Theta_2(V_{thresh} - V_{t-1}) + V_{t-1} \cdot \Theta_2'(V_{thresh} - V_{t-1})] \cdot w_{input} \quad (18)$$

If we define $\Theta_2'(x) = 0$, then the expression for an arbitrary derivative for a past x is:

$$\frac{\partial y_t}{\partial x_{t-n}} = \Theta_1'(V_t - V_{thresh}) \cdot w_{input} (1 - w_{leak})^n \prod_{i=1}^n \Theta_2(V_{thresh} - V_{t-i}) \quad (19)$$

One can see that the crucial part here is the function Θ_1 that prevents any gradient to pass. Therefore, we redefine the gradient of Θ_1 to be 1 and keep the gradient of Θ_2 as 0. This procedure is only a small change to the equations, which only affects the backpropagation step and leaves the forward propagation untouched.

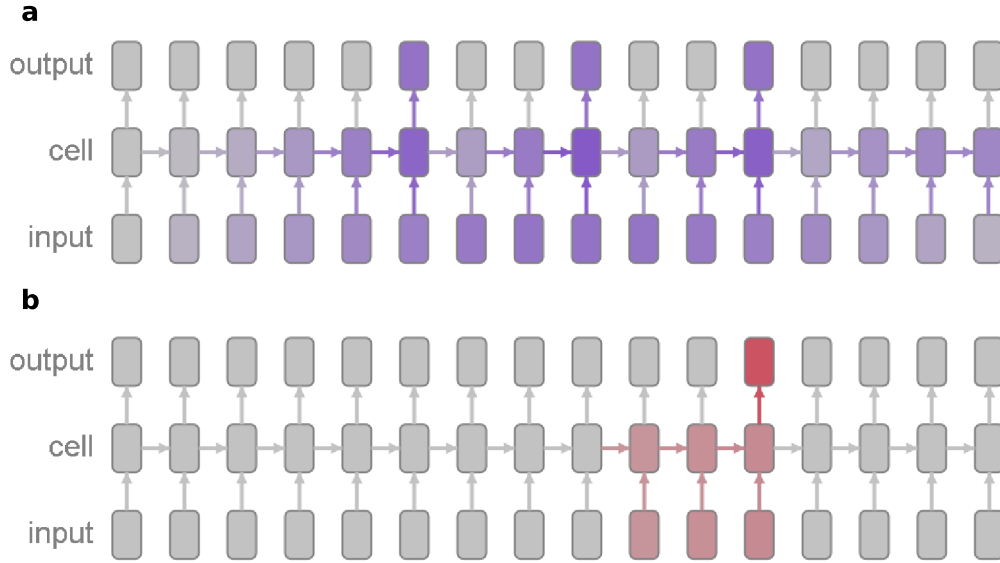


Figure 4: **The response and gradient of a LIF cell.** Each column represents one time step. The color saturation denotes the value of the cells which results from the inputs **a**. **b**, the propagated error from the red time step. The derivatives are defined as follows: $\Theta'_1(x) = 1$, $\Theta'_2(x) = 0$. For interactive version see: https://rgerum.github.io/paper_spiking_machine_intelligence/#lif_backpropagation

The gradient enters the cell (as $\Theta'_1 = 1$) and propagates to all input units that contributed to the spike (see Fig. 4) but does not penetrate to inputs that contributed to the previous spike (as $\Theta'_2 = 0$). We have shown that our gradient definition allows errors to pass the LIF neurons to pre-connected layers. For the backpropagation procedure the gradients with respect to the LIF parameters is also needed, if they are supposed to be trainable (w_{input} , w_{leak} , for complete gradients see Supplements).

In the next step, the LIF unit implementation described above is embedded in a hybrid neural network out of LSTM layers and a softmax layer. This hybrid neural network is applied to an image classification task, where 10 different flower species should be identified. We are aware of the fact that the LSTM units add further complex effects to the model, but we use them as they are a simple method to integrate the spikes and transform them into a class label. The used data set is a sub-data set of the 102 category flower data set (Nilsback and Zisserman, 2008) with only 10 categories. Thus, the LIF units should pre-process and compress the images of the different blossoms.

LIF Units for Image Classification

Network Architecture 1

The classification task on different blossoms is based on the 10 most occurring flower species (see Suppl. Fig. S2) of the 102 category flower data set (Nilsback and Zisserman, 2008). The used network consists of one LIF layer with 3 different LIF units types ($3 \times 2 = 6$ trainable parameters) compressing the colored images of 500x400 pixels.

The three LIF unit types each get exactly one color channel of the input images. In each time step each LIF unit type receives one column of one color channel of the image as input and returns a spike vector still representing the same color channel. Thus, the view that the LIF layer consists of 1200 individual LIF neurons of 3 different sorts (in analogy to network architecture 2) with 1D spike train output is equivalent, although for programming reasons the tensor notation was used in the tensorflow (Abadi et al., 2015) implementation.

Thus, the 8 bit images are compressed by a factor of 8 as each 8 bit integer is replaced by a boolean number (spike, no spike). The compressed spike data is fed to an LSTM layer (30 units) connected to a fully connected output layer with softmax activation (10 units) (see Tab. 1). As loss function the categorical cross-entropy is used. The parameters w_{input} and w_{leak} of the LIF units, as well as the LSTM and softmax parameters are trained via backpropagation.

The training procedure is stopped after 30 epochs of no improvement of the test accuracy ("early stopping"). The classification accuracy for one image (see fig. 5) is defined as the average probability value of the correct label during

Table 1: **Network architecture 1**

Layer (type)	Output Shape	Parameters #
LIF-Layer	(None, 400, 500, 3)	6
Reshape	(None, 500, 1200)	0
LSTM Layer	(None, 500, 30)	147720
Dropout	(None, 500, 30)	0
Time distributed Dense	(None, 500, 30)	930
Dropout	(None, 500, 30)	0
Softmax	(None, 500, 10)	310

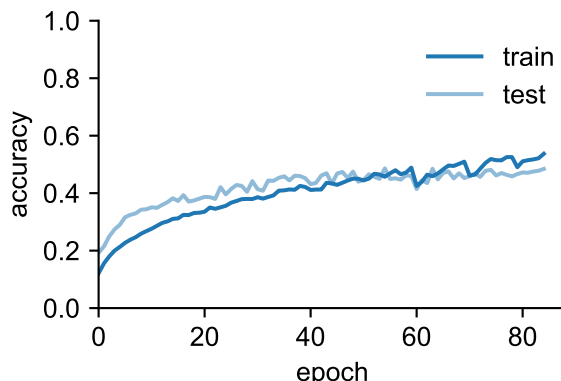


Figure 5: **Accuracy of training a network with a LIF layer.** The training accuracy is shown in dark blue and the test accuracy in light blue.

the image presentation, which is a very conservative estimator for the accuracy. The overall test accuracy (all test images) achieves a value of over 40 %, whereas the chance accuracy is 10% (10 categories). This proves that the LIF neurons can be trained via backpropagation so that they operate in a sophisticated parameter range.

Note that the data set does not allow the neural network to train on trivial features such as the color of the flower as the data set contains different color variants of the same flower species. The LIF units compress the image, nevertheless the shape of the flowers can still be seen in the spike patterns (see Fig. 6). The here described model proves that spiking layers can be trained for a classification task.

Network Architecture 2

We further provide evidence that a classification network can also be trained, when there is a fully-connected layer pre-connected to the LIF layer. Here, the LIF layer consists of 1200 LIF units, generating output spike trains (1D boolean scalar spike train). Each LIF unit receives a weighted sum of $3 \cdot 400$ values as input (3 color channels and 400 as the images consist of 400 rows). The x-coordinate (500 pixels width of the image) is the time axis.

In contrast to the architecture above (network 1), with only 6 trainable parameters except LSTM and softmax layer (3 LIF neuron types, 1200 LIF neurons), this network has 1,441,200 trainable parameters for the pre-connected fully-connected layer and 2,400 trainable parameters (w_{input} , w_{leak}) for the 1,200 individual LIF units (see Tab. 2). The fact that the

Table 2: **Network architecture 2**

Layer (type)	Output Shape	Parameters #
Reshape	(None, 500, 1200)	0
TimeDistributed Dense	(None, 500, 1200)	1441200
LIF-Layer	(None, 500, 1200)	2400
LSTM Layer	(None, 500, 30)	147720
Dropout	(None, 500, 30)	0
Time distributed Dense	(None, 500, 30)	930
Dropout	(None, 500, 30)	0
Softmax	(None, 500, 10)	310

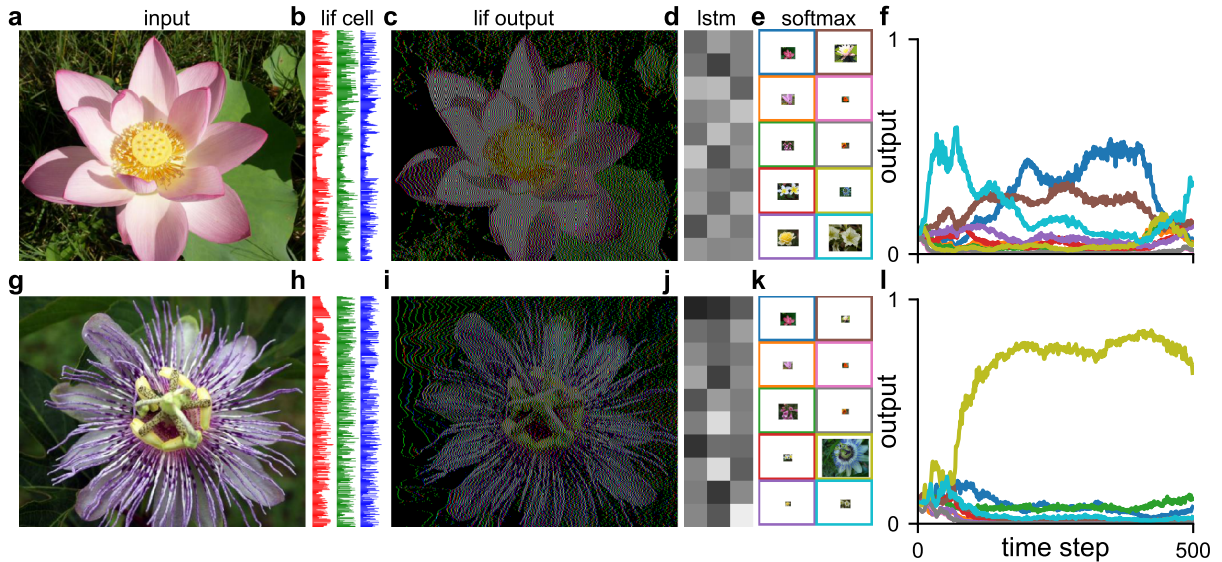


Figure 6: **Spiking network processes images.** The network takes images as input (a, g) and applies a LIF layer (b, h) to generate spike trains for each row and color channel (c, i). These spike trains are fed into an LSTM layer (d, j) which is followed by a softmax layer (e, k). The softmax layer predicts the category of the image (f, l). The three different colorbars (lif cell) represent the internal state of the LIF units for the three different color channels. The spike data produced by this LIF layer is shown under the heading lif output. The activation of the LSTM layer is shown as color map (lstm). The category probability calculated through the softmax layer is represented by the size of the category images (softmax). For interactive version see: https://rgerum.github.io/paper_spiking_machine_intelligence/#lif_network1

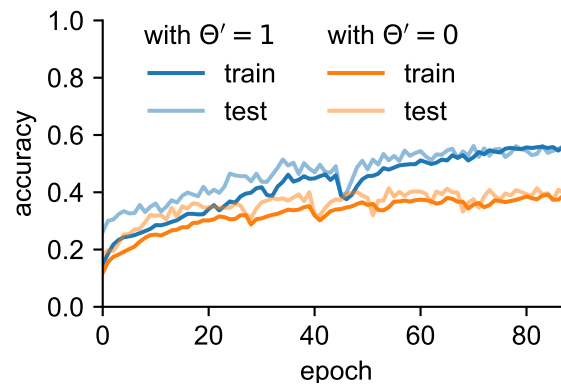


Figure 7: **Accuracy of training a network with included LIF layer.** The orange curves show the accuracy during training without manually setting the gradient of $\Theta'_1 = 1$ (disappearing gradient network, dark orange: training accuracy, light orange: test accuracy). The gradient cannot pass the LIF units. The blue curves in contrast show that the algorithm is able to train the LIF layer as well as the pre-connected dense layer (dark blue: training accuracy, light blue: test accuracy).

gradient can pass the LIF units can be seen when analyzing the accuracy as a function of the epochs (learning curve). The accuracy is higher for the LIF units with the activation function gradient ($\Theta'_1 = 1$) set to one (blue curves). This is true for training as well as test accuracy.

The test accuracy for the network, where the gradient can pass the LIF layer, is increased by more than 10 % compared to the disappearing gradient network (orange curve) and raises up to a value of approximately 55 % (see Fig. 7). Nevertheless, the accuracy of the disappearing gradient network is not at chance level, as the random connections lead to usable features for the higher layers (LSTM layers), an effect that was shown in biology as well as in computer science (see e.g. (Dasgupta et al., 2017)). In the following, we show that the output of the LIF layer significantly changes over the training epochs. Thus, the time course of the output of a LIF unit for one certain image is shown in Fig. 8.

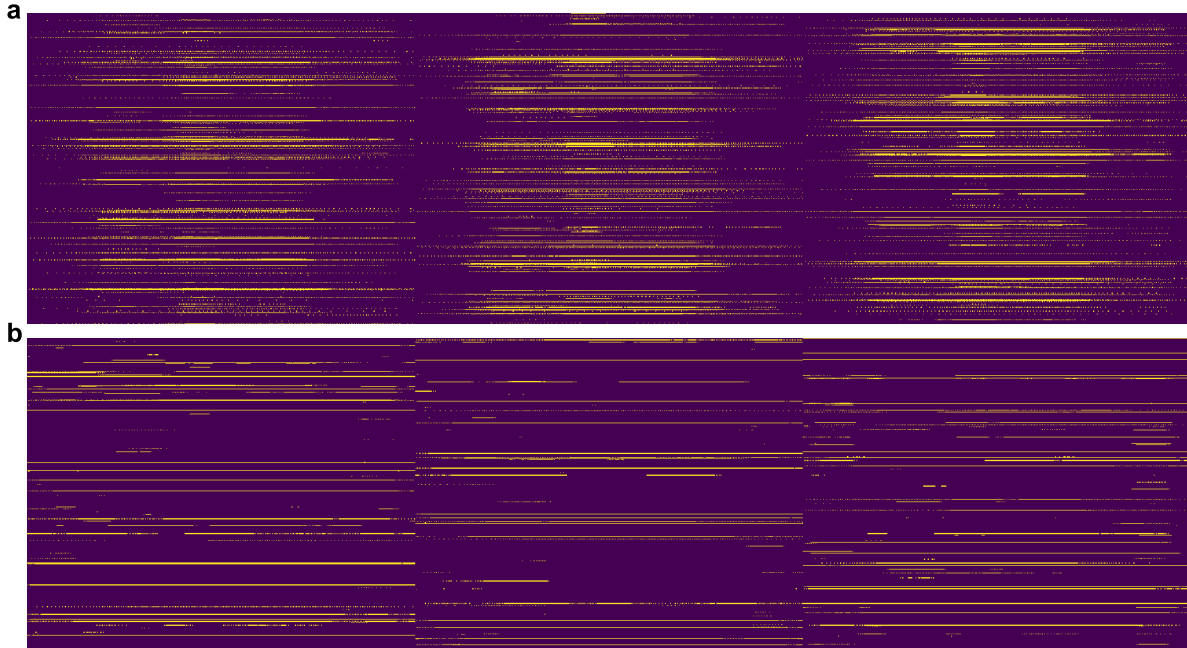


Figure 8: **Training of a network with LIF units.** **a** the spiking patterns of the LIF units before training (epoch 0, each line in the three blocks represents one of the 1200 neurons, the x-axis is the 500 time points, yellow represents a spike, purple represents no spike). **b** the spiking patterns of the LIF units after training (epoch 172). The input of one LIF unit in each time step is a weighted sum of the rows of the image (each image has 400 rows and 3 color channels, input: weighted sum of 1200 values). It can be seen that the output spike patterns change during training (**a**, epoch 0, **b** epoch 172) and that the spike density is reduced. Thus, the network develops a sparse coding of the input image. For interactive version see: https://rgerum.github.io/paper_spiking_machine_intelligence/#lif_network2

The spike patterns clearly change during the training process and the spike occurrences decreases (see Fig. 8). This effect –called sparse-coding (Olshausen and Field, 1997)– is correlated with a higher performance of the network and shows that the gradient can pass the LIF layer. Furthermore, sparse-coding of input stimuli is a basic principle in biological neural networks and here emerges automatically due to our training method.

Discussion

Summary

In this study, we have done an in-depth analysis of the maths behind, and the applicability of LIF neurons in Machine Learning.

We show that LIF units can be embedded in standard neural network models and can be trained with backpropagation. We developed a definition of the gradient, that allows the backpropagated error of a spike to be assigned to those inputs that contributed to this spike. This was done by fixing the derivatives of the activation functions ($\Theta'_1 = 1$, $\Theta'_2 = 0$).

For our analysis we chose a complex image data set, which has in contrast to simpler data sets such as MNIST, more different frequencies, which translate into different spiking patterns. Up to now, in most studies only simpler data sets were used (for review see Tavanaei et al. (2019)).

Limitations

The aim of our study was to establish a simple idea how to train neural networks consisting of LIF neurons, although we are aware of the fact that we do not yet achieve state-of-the-art performance compared to other architectures optimized for image classification (see e.g. (Xia et al., 2017; Feng et al., 2019; Qin et al., 2019)). Additionally, to achieve higher performance the recurrent neural networks have to be optimized for the used hardware components (Bhuiyan et al., 2010).

However, we are convinced that our method is a very direct and uncomplicated way to train LIF networks and thus is interesting to the Machine Learning as well as Neuroscience community. Furthermore, our method is easy to implement in existing Machine Learning frameworks such as Keras (Chollet, 2018) and thus can efficiently be run on GPU devices. The interactive visualizations help to further understand the computational mechanisms and are a step towards explainable AI. To gain a deeper understanding how Machine Learning algorithms work, i.e. to solve the black-box problem (also opacity debate), has currently become an important issue in AI research (Castelvecchi, 2016; De Laat, 2018).

The results of this study have the potential to provide novel insights in the function of biological neural networks (cf. e.g. (Schemmel et al., 2006; Jin et al., 2010)). Thus, we think that the application of analysis techniques developed for untrained or randomly connected neural networks such as stability analysis (Liapunov exponent) or motif distribution analysis (see e.g. (Bertschinger and Natschläger, 2004; Krauss et al., 2019c,a,b)), can be applied to the spiking neural networks trained with backpropagation to gain new insights in brain dynamics and function.

Concluding Remarks

The implementation of biological principles in Machine Learning such as sparsity (Gerum et al., 2020) or spiking properties can help to improve the performance of Machine Learning algorithms. Furthermore, we hypothesize that spiking neural networks unfold their full potential in tasks with serial data such as speech or music classification (Schilling et al., 2020).

Acknowledgements

We thank Nvidia for the donation of two Titan Xp Gpu devices.

References

- Abadi, M., Agarwal, A., Barham, P., Brevdo, E., Chen, Z., Citro, C., Corrado, G. S., Davis, A., Dean, J., Devin, M., Ghemawat, S., Goodfellow, I., Harp, A., Irving, G., Isard, M., Jia, Y., Jozefowicz, R., Kaiser, L., Kudlur, M., Levenberg, J., Mané, D., Monga, R., Moore, S., Murray, D., Olah, C., Schuster, M., Shlens, J., Steiner, B., Sutskever, I., Talwar, K., Tucker, P., Vanhoucke, V., Vasudevan, V., Viégas, F., Vinyals, O., Warden, P., Wattenberg, M., Wicke, M., Yu, Y., and Zheng, X. (2015). TensorFlow: Large-scale machine learning on heterogeneous systems. Software available from tensorflow.org.
- Abadi, M., Barham, P., Chen, J., Chen, Z., Davis, A., Dean, J., Devin, M., Ghemawat, S., Irving, G., Isard, M., et al. (2016). Tensorflow: A system for large-scale machine learning. In *12th {USENIX} symposium on operating systems design and implementation ({OSDI} 16)*, pages 265–283.
- Atkinson, K. E. (1989). An introduction to numerical analysis. new york: John willey & sons.
- Bertschinger, N. and Natschläger, T. (2004). Real-time computation at the edge of chaos in recurrent neural networks. *Neural computation*, 16(7):1413–1436.
- Bhuiyan, M. A., Pallipuram, V. K., Smith, M. C., Taha, T., and Jalasutram, R. (2010). Acceleration of spiking neural networks in emerging multi-core and gpu architectures. In *2010 IEEE International Symposium on Parallel & Distributed Processing, Workshops and Phd Forum (IPDPSW)*, pages 1–8. IEEE.
- Bohte, S. M., Kok, J. N., and La Poutré, J. A. (2000). Spikeprop: backpropagation for networks of spiking neurons. In *ESANN*, volume 48, pages 17–37.
- Bostock, M., Ogievetsky, V., and Heer, J. (2011). D³ data-driven documents. *IEEE transactions on visualization and computer graphics*, 17(12):2301–2309.
- Burkitt, A. N. (2006). A review of the integrate-and-fire neuron model: I. homogeneous synaptic input. *Biological cybernetics*, 95(1):1–19.
- Castelvecchi, D. (2016). Can we open the black box of ai? *Nature News*, 538(7623):20.
- Chollet, F. (2018). *Deep Learning mit Python und Keras: Das Praxis-Handbuch vom Entwickler der Keras-Bibliothek*. MITP-Verlags GmbH & Co. KG.
- Dasgupta, S., Stevens, C. F., and Navlakha, S. (2017). A neural algorithm for a fundamental computing problem. *Science*, 358(6364):793–796.
- De Laat, P. B. (2018). Algorithmic decision-making based on machine learning from big data: Can transparency restore accountability? *Philosophy & technology*, 31(4):525–541.

- Dominguez-Morales, J. P., Jimenez-Fernandez, A., Rios-Navarro, A., Cerezuela-Escudero, E., Gutierrez-Galan, D., Dominguez-Morales, M. J., and Jimenez-Moreno, G. (2016). Multilayer spiking neural network for audio samples classification using spinnaker. In *International Conference on Artificial Neural Networks*, pages 45–53. Springer.
- Feng, J., Wang, Z., Zha, M., and Cao, X. (2019). Flower recognition based on transfer learning and adam deep learning optimization algorithm. In *Proceedings of the 2019 International Conference on Robotics, Intelligent Control and Artificial Intelligence*, pages 598–604.
- Field, G. D., Uzzell, V., Chichilnisky, E., and Rieke, F. (2019). Temporal resolution of single-photon responses in primate rod photoreceptors and limits imposed by cellular noise. *Journal of neurophysiology*, 121(1):255–268.
- Gerum, R. (2020). pylustrator: code generation for reproducible figures for publication. *Journal of Open Source Software*, 5(51):1989.
- Gerum, R. C., Erpenbeck, A., Krauss, P., and Schilling, A. (2020). Sparsity through evolutionary pruning prevents neuronal networks from overfitting. *Neural Networks*.
- Gross, G. W. and Kowalski, J. M. (1999). Origins of activity patterns in self-organizing neuronal networks in vitro. *Journal of Intelligent Material Systems and Structures*, 10(7):558–564.
- Hassabis, D., Kumaran, D., Summerfield, C., and Botvinick, M. (2017). Neuroscience-inspired artificial intelligence. *Neuron*, 95(2):245–258.
- Herculano-Houzel, S. (2009). The human brain in numbers: a linearly scaled-up primate brain. *Frontiers in human neuroscience*, 3:31.
- Hochreiter, S. and Schmidhuber, J. (1997). Long short-term memory. *Neural computation*, 9(8):1735–1780.
- Hodgkin, A. L. and Huxley, A. F. (1952). A quantitative description of membrane current and its application to conduction and excitation in nerve. *The Journal of physiology*, 117(4):500–544.
- Hunter, J. D. (2007). Matplotlib: A 2d graphics environment. *Computing in science & engineering*, 9(3):90–95.
- Izhikevich, E. M. and FitzHugh, R. (2006). Fitzhugh-nagumo model. *Scholarpedia*, 1(9):1349.
- Jin, X., Lujan, M., Plana, L. A., Davies, S., Temple, S., and Furber, S. B. (2010). Modeling spiking neural networks on spinnaker. *Computing in science & engineering*, 12(5):91–97.
- Kheradpisheh, S. R. and Masquelier, T. (2019). S4nn: temporal backpropagation for spiking neural networks with one spike per neuron. *arXiv preprint arXiv:1910.09495*.
- Kim, R., Li, Y., and Sejnowski, T. J. (2019). Simple framework for constructing functional spiking recurrent neural networks. *Proceedings of the national academy of sciences*, 116(45):22811–22820.
- Koch, C., Segev, I., et al. (1998). *Methods in neuronal modeling: from ions to networks*. MIT press.
- Koopman, A., Van Leeuwen, M., and Vreeken, J. (2003). Dynamic neural networks, comparing spiking circuits and lstm.
- Krauss, P., Metzner, C., Schilling, A., Schütz, C., Tziridis, K., Fabry, B., and Schulze, H. (2017). Adaptive stochastic resonance for unknown and variable input signals. *Scientific reports*, 7(1):1–8.
- Krauss, P., Metzner, C., Schilling, A., Tziridis, K., Traxdorf, M., Wollbrink, A., Rampp, S., Pantev, C., and Schulze, H. (2018). A statistical method for analyzing and comparing spatiotemporal cortical activation patterns. *Scientific reports*, 8(1):1–9.
- Krauss, P., Prebeck, K., Schilling, A., and Metzner, C. (2019a). Recurrence resonance” in three-neuron motifs. *Frontiers in computational neuroscience*, 13.
- Krauss, P., Schuster, M., Dietrich, V., Schilling, A., Schulze, H., and Metzner, C. (2019b). Weight statistics controls dynamics in recurrent neural networks. *PloS one*, 14(4):e0214541.
- Krauss, P., Tziridis, K., Metzner, C., Schilling, A., Hoppe, U., and Schulze, H. (2016). Stochastic resonance controlled upregulation of internal noise after hearing loss as a putative cause of tinnitus-related neuronal hyperactivity. *Frontiers in neuroscience*, 10:597.
- Krauss, P., Zankl, A., Schilling, A., Schulze, H., and Metzner, C. (2019c). Analysis of structure and dynamics in three-neuron motifs. *Frontiers in Computational Neuroscience*, 13:5.
- Kriegeskorte, N. and Douglas, P. K. (2018). Cognitive computational neuroscience. *Nature neuroscience*, 21(9):1148–1160.
- Lee, C., Sarwar, S. S., Panda, P., Srinivasan, G., and Roy, K. (2020). Enabling spike-based backpropagation for training deep neural network architectures. *Frontiers in Neuroscience*, 14.

- Mar, R. A. (2004). The neuropsychology of narrative: Story comprehension, story production and their interrelation. *Neuropsychologia*, 42(10):1414–1434.
- Nilsback, M.-E. and Zisserman, A. (2008). Automated flower classification over a large number of classes. In *2008 Sixth Indian Conference on Computer Vision, Graphics & Image Processing*, pages 722–729. IEEE.
- Olshausen, B. A. and Field, D. J. (1997). Sparse coding with an overcomplete basis set: A strategy employed by v1? *Vision research*, 37(23):3311–3325.
- Perkel, D. H. and Bullock, T. H. (1968). Neural coding. *Neurosciences Research Program Bulletin*.
- Pontes-Filho, S. and Nichele, S. (2019). Towards a framework for the evolution of artificial general intelligence. *arXiv preprint arXiv:1903.10410*.
- Pozzi, I., Nusselder, R., Zambrano, D., and Bohté, S. (2018). Gating sensory noise in a spiking subtractive lstm. In *International Conference on Artificial Neural Networks*, pages 284–293. Springer.
- Qin, M., Xi, Y., and Jiang, F. (2019). A new improved convolutional neural network flower image recognition model. In *2019 IEEE Symposium Series on Computational Intelligence (SSCI)*, pages 3110–3117. IEEE.
- Rezaabad, A. L. and Vishwanath, S. (2020). Long short-term memory spiking networks and their applications. *arXiv preprint arXiv:2007.04779*.
- Rieke, F. and Baylor, D. A. (1998). Single-photon detection by rod cells of the retina. *Reviews of Modern Physics*, 70(3):1027.
- Russakovsky, O., Deng, J., Su, H., Krause, J., Satheesh, S., Ma, S., Huang, Z., Karpathy, A., Khosla, A., Bernstein, M., et al. (2015). Imagenet large scale visual recognition challenge. *International journal of computer vision*, 115(3):211–252.
- Schemmel, J., Grubl, A., Meier, K., and Mueller, E. (2006). Implementing synaptic plasticity in a vlsi spiking neural network model. In *The 2006 IEEE International Joint Conference on Neural Network Proceedings*, pages 1–6. IEEE.
- Schilling, A., Gerum, R., Zankl, A., Schulze, H., Metzner, C., and Krauss, P. (2020). Intrinsic noise improves speech recognition in a computational model of the auditory pathway. *bioRxiv*.
- Schrauwen, B. and Van Campenhout, J. (2004a). Extending spikeprop. In *2004 IEEE International Joint Conference on Neural Networks (IEEE Cat. No. 04CH37541)*, volume 1, pages 471–475. IEEE.
- Schrauwen, B. and Van Campenhout, J. (2004b). Improving spikeprop: Enhancements to an error-backpropagation rule for spiking neural networks. In *Proceedings of the 15th ProRISC workshop*, volume 11, pages 301–305.
- Sheng, Y.-B. and Zhou, L. (2017). Distributed secure quantum machine learning. *Science Bulletin*, 62(14):1025–1029.
- Shevlin, H., Vold, K., Crosby, M., and Halina, M. (2019). The limits of machine intelligence: Despite progress in machine intelligence, artificial general intelligence is still a major challenge. *EMBO reports*, 20(10):e49177–e49177.
- Steinkraus, D., Buck, I., and Simard, P. (2005). Using gpus for machine learning algorithms. In *Eighth International Conference on Document Analysis and Recognition (ICDAR’05)*, pages 1115–1120. IEEE.
- Tavanaei, A., Ghodrati, M., Kheradpisheh, S. R., Masquelier, T., and Maida, A. (2019). Deep learning in spiking neural networks. *Neural Networks*, 111:47–63.
- Tenenbaum, J. B., Griffiths, T. L., and Kemp, C. (2006). Theory-based bayesian models of inductive learning and reasoning. *Trends in cognitive sciences*, 10(7):309–318.
- Thorpe, S., Delorme, A., and Van Rullen, R. (2001). Spike-based strategies for rapid processing. *Neural networks*, 14(6-7):715–725.
- Walt, S. v. d., Colbert, S. C., and Varoquaux, G. (2011). The numpy array: a structure for efficient numerical computation. *Computing in science & engineering*, 13(2):22–30.
- Wu, Y., Deng, L., Li, G., Zhu, J., and Shi, L. (2018). Spatio-temporal backpropagation for training high-performance spiking neural networks. *Frontiers in neuroscience*, 12:331.
- Xia, X., Xu, C., and Nan, B. (2017). Inception-v3 for flower classification. In *2017 2nd International Conference on Image, Vision and Computing (ICIVC)*, pages 783–787. IEEE.

Supplementary Material

Firing Rates

We will analytically calculate the number of timesteps with a constant input I which are necessary to provoke a spike. At time t_0 we start with $V_{t_0} = w_{input} \cdot I$ and apply the update rule for LIF units as shown above:

$$V_{t_n} = w_{input} \cdot I + (1 - w_{leak}) \cdot V_{t_{n-1}} \quad (20)$$

The implicit description of V_{t_n} can be written in an explicit manner.

$$V_{t_n} = \sum_{i=0}^n (1 - w_{leak})^i \cdot w_{input} \cdot I \quad (21)$$

The criterion for a spike is: $V_{t_n} \geq V_{thresh}$. Thus, the following inequation has to be solved:

$$V_{thresh} \leq \sum_{i=0}^n (1 - w_{leak})^i \cdot w_{input} \cdot I \quad (22)$$

$$\leq w_{input} \cdot I \cdot \sum_{i=0}^n (1 - w_{leak})^i \quad \text{with } \sum_{i=0}^n a^i = \frac{a^{n+1} - 1}{a - 1} \quad (23)$$

$$\leq w_{input} \cdot I \cdot \frac{(1 - w_{leak})^{n+1} - 1}{-w_{leak}} \quad (24)$$

$$-\frac{V_{thresh}}{I} \cdot \frac{w_{leak}}{w_{input}} + 1 \geq (1 - w_{leak})^{n+1} \quad (25)$$

$$\ln \left(-\frac{V_{thresh}}{I} \cdot \frac{w_{leak}}{w_{input}} + 1 \right) \geq (n + 1) \cdot \ln(1 - w_{leak}) \quad (26)$$

$$n \geq \frac{\ln \left(1 - \frac{V_{thresh}}{I} \cdot \frac{w_{leak}}{w_{input}} \right)}{\ln(1 - w_{leak})} - 1 \quad (27)$$

$$(28)$$

This results in the number of timesteps until the next spike event.

$$n = \text{ceil} \left(\frac{\ln \left(1 - \frac{V_{thresh}}{I} \cdot \frac{w_{leak}}{w_{input}} \right)}{\ln(1 - w_{leak})} - 1 \right) \quad (29)$$

Note, for $w_{leak} = 0$ this simplifies to:

$$n = \text{ceil} \left(\frac{V_{thresh}}{w_{input} \cdot I} \right) \quad (30)$$

The equation shows that n is a nonlinear function of w_{leak} and w_{input} and thus a simple downregulation of w_{leak} cannot be compensated by a downregulation of w_{input} . On the other hand, V_{thresh} can be fixed to 1 without loss of generality as a change of V_{thresh} can be absorbed in w_{input} .

The spiking only occurs at all if the input exceeds the input threshold:

$$I_{min} = \frac{V_{thresh} \cdot w_{leak}}{w_{input}} \quad (31)$$

Smaller inputs lead to a divergence of the n as the cell state decays faster than it is resupplied by the input. The equation for the input threshold I_{min} shows that the input threshold is only non-zero if the neuron is "leaky", e.g. has a leak parameter $w_{leak} \neq 0$.

The fact that the two parameters w_{leak} and w_{input} have different effects on the spike rate, and cannot be trivially combined to one parameter, training of these two parameters can help to extract interesting features from the input data.

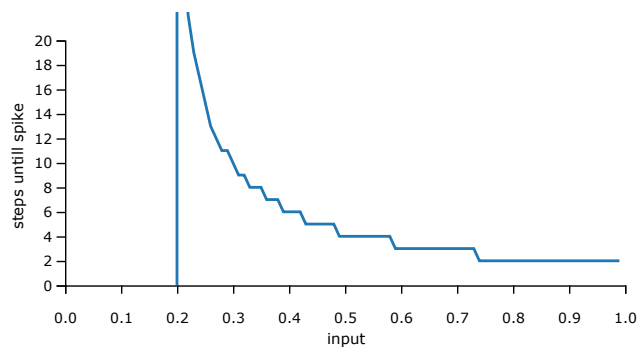


Figure S1: **Average number of timesteps needed for spike (corresponds to inverse spike rate).** The curve (blue) shows the steps it takes for the neuron to spike when it receives a constant input ($w_{\text{input}} = 0.5$, $w_{\text{leak}} = 0.1$).

Limited image data set

The neural networks used in this study were trained on the classification of 10 different flower species, which are a subset of 102 Oxford flower data set (Nilsback and Zisserman, 2008).

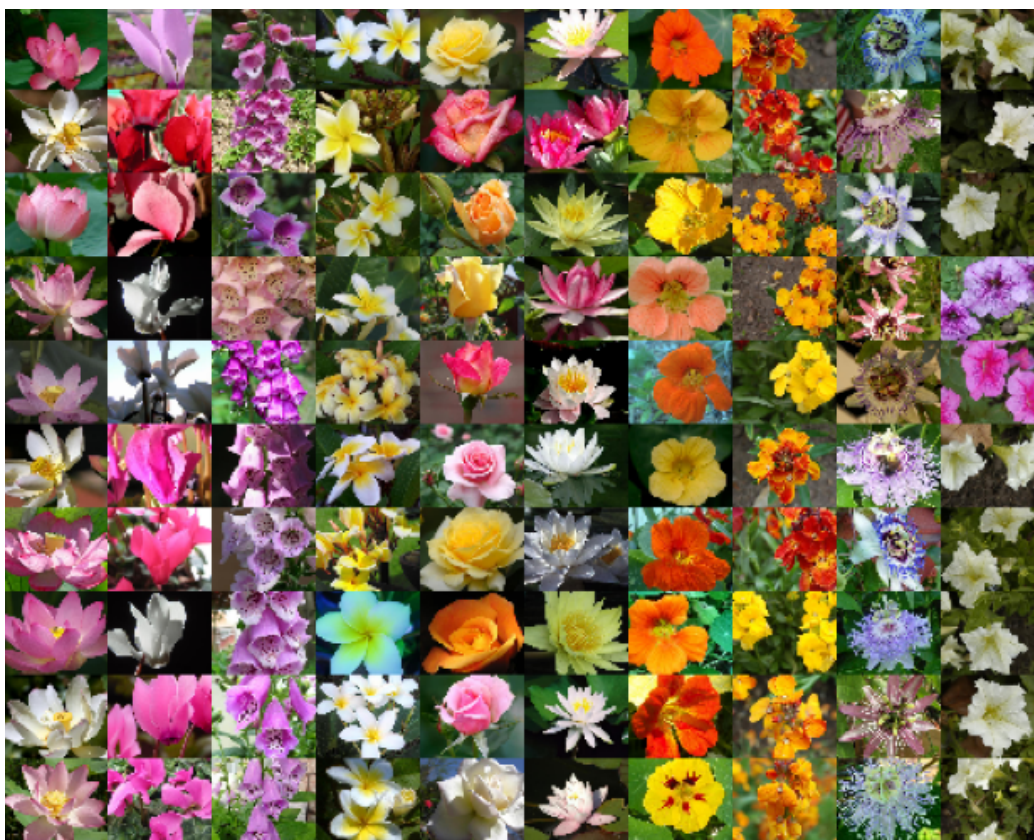


Figure S2: **Exemplary images from the limited data set with 10 categories out of 102 Oxford flower data set**

Gradients

The gradient with respect to w_{input} :

$$\begin{aligned}
 \frac{dy_t}{dw_{\text{input}}} &= \frac{\partial y_t}{\partial V_t} \left(\frac{\partial V_t}{\partial w_{\text{input}}} + \frac{\partial V_t}{\partial V_{t-1}} \frac{dV_{t-1}}{dw_{\text{input}}} \right) = \\
 & \frac{\partial y_t}{\partial V_t} \left\{ \frac{\partial V_t}{\partial w_{\text{input}}} + \frac{\partial V_t}{\partial V_{t-1}} \left[\frac{\partial V_{t-1}}{\partial w_{\text{input}}} + \frac{\partial V_{t-1}}{\partial V_{t-2}} \left(\frac{\partial V_{t-2}}{\partial w_{\text{input}}} + \frac{\partial V_{t-2}}{\partial V_{t-3}} \frac{dV_{t-3}}{dw_{\text{input}}} \right) \right] \right\} = \\
 & \Theta'_1(V_t - V_{\text{thresh}}) \cdot \left[x_t + (1 - w_{\text{leak}}) \Theta_2(V_{\text{thresh}} - V_{t-1}) x_{t-1} + \right. \\
 & (1 - w_{\text{leak}})^2 \Theta_2(V_{\text{thresh}} - V_{t-1}) \Theta_2(V_{\text{thresh}} - V_{t-2}) x_{t-2} + \\
 & \left. (1 - w_{\text{leak}})^3 \Theta_2(V_{\text{thresh}} - V_{t-1}) \Theta_2(V_{\text{thresh}} - V_{t-2}) \Theta_2(V_{\text{thresh}} - V_{t-3}) \frac{dV_{t-3}}{dw_{\text{input}}} \right] = \\
 & \Theta'_1(V_t - V_{\text{thresh}}) \cdot \left[x_t + \sum_{n=1}^N x_{t-n} (1 - w_{\text{leak}})^n \cdot \prod_{i=1}^n \Theta_2(V_{\text{thresh}} - V_{t-i}) \right]
 \end{aligned} \tag{32}$$

The gradient with respect to w_{leak} :

$$\begin{aligned}
 \frac{dy_t}{dw_{\text{leak}}} &= \frac{\partial y_t}{\partial w_{\text{leak}}} \frac{dV_t}{dw_{\text{leak}}} = \\
 &= \Theta'_1(V_t - V_{\text{thresh}}) \cdot \\
 & \left[-V_{t-1} \Theta_2(V_{\text{thresh}} - V_{t-1}) - V_{t-2} (1 - w_{\text{leak}}) \Theta_2(V_{\text{thresh}} - V_{t-1}) \Theta_2(V_{\text{thresh}} - V_{t-2}) - \right. \\
 & V_{t-3} (1 - w_{\text{leak}})^2 \Theta_2(V_{\text{thresh}} - V_{t-1}) \Theta_2(V_{\text{thresh}} - V_{t-2}) \Theta_2(V_{\text{thresh}} - V_{t-3}) + \\
 & \left. (1 - w_{\text{leak}})^3 \Theta_2(V_{\text{thresh}} - V_{t-1}) \Theta_2(V_{\text{thresh}} - V_{t-2}) \Theta_2(V_{\text{thresh}} - V_{t-3}) \frac{dV_{t-3}}{dw_{\text{leak}}} \right] = \\
 & \Theta'_1(V_t - V_{\text{thresh}}) \cdot \left[-\sum_{n=1}^N V_{t-n} (1 - w_{\text{leak}})^{n-1} \cdot \prod_{i=1}^n \Theta_2(V_{\text{thresh}} - V_{t-i}) \right]
 \end{aligned} \tag{33}$$

Keras Implementation

These gradient definitions can be implemented with the following code in tensorflow:

```

@tf.function
def lif_gradient(x, w_i, w_l, t_thresh=1):
    time_steps = x.shape[1]

    Vm = w_i * x[:, 0]
    states = tf.TensorArray(tf.float32, size=time_steps)

    for i in tf.range(time_steps):
        Vm = w_i * x[:, i] + (1 - w_l) * Vm * theta2(t_thresh - Vm)
        spike = theta1(Vm - t_thresh)
        states = states.write(i, spike)

    return tf.transpose(states.stack())
    
```

With the theta functions defined as:

```

@tf.custom_gradient
def theta2(x):
    def grad(dy):
        return dy*0
    return tf.cast(x > 0, tf.float32), grad

@tf.custom_gradient
def theta1(x):
    def grad(dy):
        return dy*1
    return tf.cast(x > 0, tf.float32), grad
    
```